Journal of Marine Science and Technology (2019) 24:297–305
https://doi.org/10.1007/s00773-018-0558-y

ORIGINAL ARTICLE

Investigation and optimization of appendage influence on the hydrodynamic performance of AUVs

Yaxing Wang[1] · Ting Gao[2] · Yongjie Pang[2] · Yuangui Tang[1]

Received: 13 November 2017 / Accepted: 16 May 2018 / Published online: 21 May 2018

Abstract
Navigational range is an important attribute of autonomous underwater vehicles (AUVs), and drag reduction efforts have been pursued to improve overall efficiency. Improved efficiency results in a more capable vehicle over all. Historically, the majority of research focused on drag reduction has been concentrated on the optimization of vehicle hull geometry. The influence of the hull appendages on drag, however, has been largely ignored owing to their smaller size. In this study, the impacts of appendage size and position on vehicle drag are investigated using a computational fluid dynamics method. The results indicate that appendages increase more drag because of their impact on the development of turbulence. The investigation of the interactions between multiple appendages fixed on a vehicle hull shows that optimization is necessary for drag reduction. This paper presents an arrangement optimization method for AUV appendages based on the Kriging approximation model and the multi-island genetic algorithm. The results of the optimization show that appendage influence on hydrodynamic performance is directly proportional to its size, and that a distributed arrangement is beneficial for drag reduction.

Keywords Computational fluid dynamics · Hydrodynamics · Underwater vehicles · Drag

1 Introduction

Autonomous underwater vehicles (AUVs) can operate independently in unpredictable ocean environments through the use of unmanned control systems and wireless communication technology. They have a broad scope of use in both civilian and military applications owing to their important role in ocean resource exploration and development.

Drag performance is critical to the navigational range of AUVs. An AUV with smaller drag can execute more assignments and save more energy to finish tasks such as detecting and tracking. Historically, the majority of research has focused on optimizing the main hull to reduce drag [1–6]. However, modern AUVs have to carry equipment for communication or detection. As a result of this demanding activity, some of these devices have to be stowed outside of the main hull. It then follows that the smaller the AUV, the smaller its hull, and the greater quantity of equipment that must be stowed externally. This externally stowed equipment has an influence on the hydrodynamic performance of the AUV, especially in regards to direct drag performance. According to the test results obtained by Allen et al. [7], when the REMUS underwater vehicle navigated at a speed of 3 kn, the drag generated by the acoustic Doppler current profiler (ADCP) accounted for 27.4% of the total drag. This value is almost equally matched with the drag generated by bare hull. Current research on AUV appendage arrangement focuses only on a simple assessment of a designed layout, and its reference value is too small for the design of a new AUV.

In this study, the accuracy of the computational fluid dynamics (CFD) method is first validated in Sect. 2 using test data from the SUBOFF model. The effects of appendage size and position on the drag of an AUV are then studied in Sect. 3. An approximate model is established between arrangement parameters and their corresponding drag values, and then optimization is conducted to reduce the AUV drag. According to results calculated by CFD simulation, the overall vehicle navigational range is improved by 6%.

✉ Yaxing Wang
wangyaxing@sia.cn

[1] State key Laboratory of Robotics, Shenyang Institute of Automation, Chinese Academy of Sciences, Shenyang 110016, China

[2] Science and Technology on Underwater Vehicle Laboratory, Harbin Engineering University, Harbin 150001, China

2 CFD validation

2.1 CFD simulation of SUBOFF

The SUBOFF model was specifically designed by the Defense Advanced Research Projects Agency (DARPA) to verify the accuracy of CFD simulations. The overall length of SUBOFF model is 4.356 m, while the maximum diameter is 0.508 m. The submarine has been built as two geometrically identical models: 5470 and 5471 [8], whose linear scale ratio is 24. The former was used for a towing tank test, and the latter was used as a wind tunnel test model. The David Taylor Model Basin (DTMB), located in the United States of America, was utilized to complete the towing tank tests with the 5470 model. The open source code library, OpenFOAM [9], is used to simulate the towing test performed with the SUBOFF model, and the results are compared with the results of this experiment. OpenFOAM is an object-oriented open-source CFD library based on the finite volume method. The analysis in this study uses the snappyHexMesh utility in OpenFOAM to generate three-dimensional meshes. The module has the ability to control the parameters used for mesh generation. Parameter variations will produce corresponding grid changes. The greatest strength of the strategy used by snappyHexMesh is that it generates predominantly hexahedral meshes with minimal cell skewness. Additionally, body fitted technology used to change the configuration of grid nodes and increase density, in the calculation of nearby objects only. Moreover, prism layers can be easily generated according to the needs of designers. The mesh generated by snappyHexMesh is shown in Fig. 1. The calculation domain is a cuboid around SUBOFF, the inlet boundary is positioned 2L upstream, and the pressure outlet condition is defined 4L downstream. The generated grid has about 9 million grid cells. The y^+ value, which is the non-dimensional normal distance to the hull surface from the first grid, is approximately between 30 and 100.

In this study, the unsteady Reynolds-averaged Navier–Stokes (URANS) approach was used to conduct simulations. To satisfy the requirement that solving time advancing faster than physical disturbance speed, the time step is set as an automatic adjustment. The adjusting law requires the Courant number to be less than 1. That is, for any grid in the flow field, the time step, Δt, should satisfy:

$$\mathrm{Co} = \frac{\Delta t|u|}{\Delta x} < 1,$$

where Co is Courant number, $|u|$ is the fluid velocity through the mesh, and Δx is the grid length along the flow direction. In this study, the PIMPLE algorithm is used to deal with the coupling of pressure and velocity in the URANS equation. The PIMPLE algorithm is a combination of the semi-implicit method for pressure linked equations (SIMPLE) algorithm and the pressure implicit with splitting of operator (PISO) algorithm. Its basic principle is that each time step is taken as a steady flow, and the simple steady-state algorithm is used to solve equations. In the last step of the solution, the PISO method is used to advance to the next time step. If the flow changes dramatically between the two time steps, the sub-relaxation method is employed to control it.

2.2 Validation of CFD simulation

Drag values for the SUBOFF model at speeds of 1.50, 2.57, 3.05, 5.14, and 6.10 m/s were calculated with the introduced method. The speed range for most AUVs ranges from 3 to 5 kn; therefore, the first two speeds were used for appendage optimization for subsequent chapters, and the last three speeds were used to verify the accuracy of the calculation method. Works by Wu [10] and Dantas and Barros [11], and our previous investigation [6, 12] were referred to conducted the validation procedure. As shown in Fig. 2, the CFD calculated values are consistent with the experimental results [13] at the last three speeds, the relative errors are within 3%. Figure 3 shows a comparison between the CFD calculations and the experimental values for the hull surface

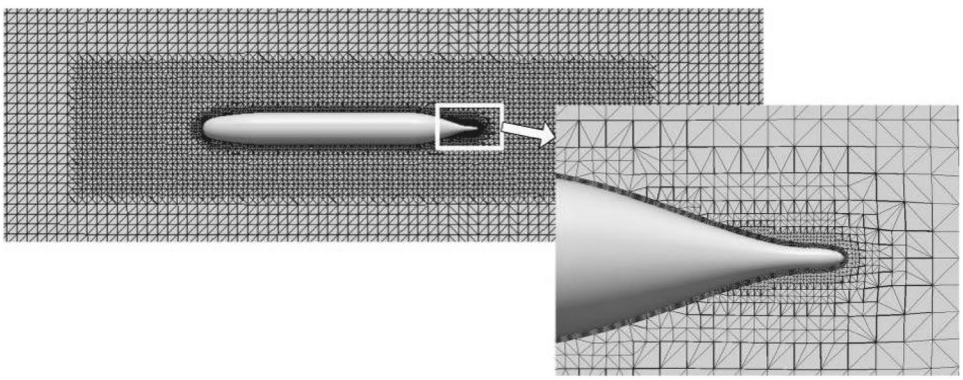

Fig. 1 Hexahedral mesh generated by snappyHexMesh

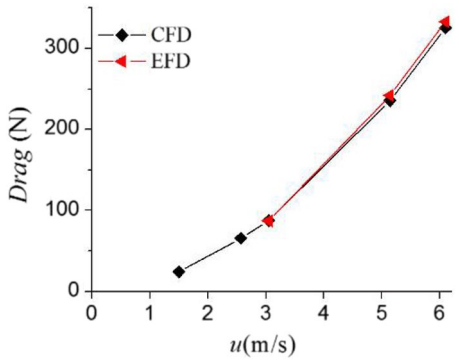

Fig. 2 Drag curve of the SUBOFF model

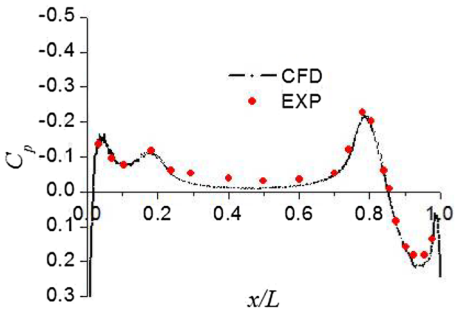

Fig. 3 The change in pressure coefficient along the SUBOFF model hull surface

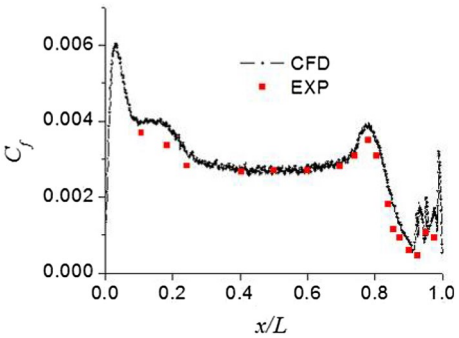

Fig. 4 The change in friction coefficient along the SUBOFF model hull surface

pressure changes when the velocity is 3.05 m/s. Figure 4 shows the results of the SUBOFF hull surface friction drag coefficient comparison between the CFD simulation values and the experimental values. From the computational results, we can see that the CFD simulation of the SUBOFF drag value is consistent with the experimental results, and also that the distribution of surface pressure coefficient and the friction coefficient. The simulation results validated that the CFD simulation results can provide a valuable reference for related research.

3 Single appendage influence on AUV hydrodynamic performance

3.1 Numerical model

Based on the previously validated simulation method, additional cylindrical appendages of different sizes were separately added into the simulation in different positions. The effects of size, height, and location on the overall hydrodynamic performance of the SUBOFF model were systematically analyzed. A successful analysis would serve as a useful reference for AUV pre-design. To make the analysis more representative and comprehensive, four locations: $x = 0.2$, 0.4, 0.6, 0.8 l ($l = 4.356$ m), four cylinder sizes: $d_{app} = 0.1$, 0.2, 0.3, 0.4d ($d = 0.508$ m), and five appendage heights: $h_{app} = 0.05$, 0.1, 0.15, 0.2, 0.3d, were investigated. The grid is illustrated in Fig. 5.

3.2 Calculation results

Figure 6 shows an increase in drag resulting from different appendage arrangements compared with the bare hull condition at two different flow speeds: 1.5 and 2.57 m/s. According to the simulation results, drag variation shows that the same tendency at different speeds that could be summarized.

The variation in total drag is the same at two different flow speeds. While all other conditions are the same, the velocity variation leads to the same percentage increase in drag. For the same appendage, when the mounting position changes from bow to stern, the hull drag will reduce to some extent and then increase later. The larger the appendage

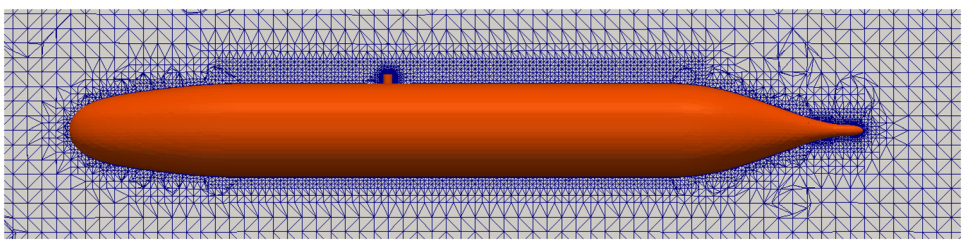

Fig. 5 Computational grid of SUBOFF model

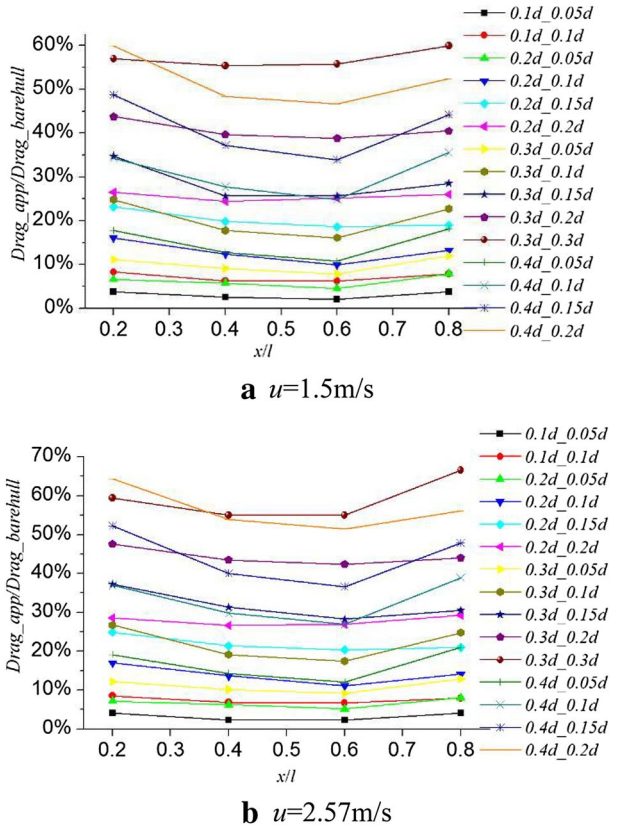

Fig. 6 Drag increase of the SUBOFF model with different appendages

diameter, the more obvious this variation law becomes. For example, the appendage diameter, $d_{app}=0.2d$, and outrigger height, $h_{app}=0.2d$, mounted in four positions, $x=0.2$, 0.4, 0.6, 0.8 l, can result in direct drag increasing by 26.5, 24.4, 25.2, and 26.0%, respectively. For the same appendage, with increase in its out-reaching height, the drag variation follows a linear law approximately. An appendage with $d_{app}=0.3d$ and location $x=0.2l$ can cause the drag to increase by 11.2, 24.8, 34.7, 43.8, and 57.0% when the out-reaching height of appendage h_{app} is 0.05, 0.1, 0.15, 0.2, and 0.3d, respectively.

For most arrangement schemes, the lift and pitching moments are small. For instance, a rudder with an area of 0.03 m^2 mounted on the stern of a ship can counter act those moments with rudder angle less than 1°. Plans that $d_{app}=0.3d$, $h_{app}=0.3d$, $x=0.8$ l and $d_{app}=0.4d$, $h_{app}=0.2d$, $x=0.8$ l have special results. The lift and pitching moments oscillate within a large range, which indicates that those arrangements produce unstable, turbulent flow. The Q criterion is the vorticity squared minus the shear strain rate squared, it is used to visualize the resolved turbulence structures. It is defined as:

$$Q=\frac{1}{2}(W_{ij}W_{ij}-S_{ij}S_{ij}),$$

where $W_{ij}=\frac{u_{i,j}-u_{j,i}}{2}$, $S_{ij}=\frac{u_{i,j}+u_{j,i}}{2}$. If Q is positive, its corresponding ISO surface is indicating distribution of vortex. Unstable turbulent flow as shown in Fig. 7, in which different color of the ISO surface is velocity vibration, can have very negative influence on AUV stability. Therefore, when designing an AUV, appendages with larger diameters and higher out-reaching should not be positioned at the rear end of the hull.

4 Calculation and optimization of the AUV drag with multiple appendages

Analysis of the influence of appendages on AUV hydrodynamic performance will help designers predict changes in the overall performance of an AUV after adding appendages. However, when designing an actual AUV, the shape of the appendages is not always cylindrical, and there may not be only one appendage. When the quantity and the shape of the appendages have been determined, designers can develop an approximate model to compare the appendage position and drag with the experimental design. Then, the model is used to perform the optimization to obtain a proper layout program for appendage arrangement with the minimum direct drag.

4.1 Calculation model

As shown in Fig. 8, a large depth AUV is selected as the computing object. Its total length, diameter, and design cruising speed are 5.6 m, 0.82 m, and 1.5 m/s, respectively. Because of the practical application requirement, the AUV

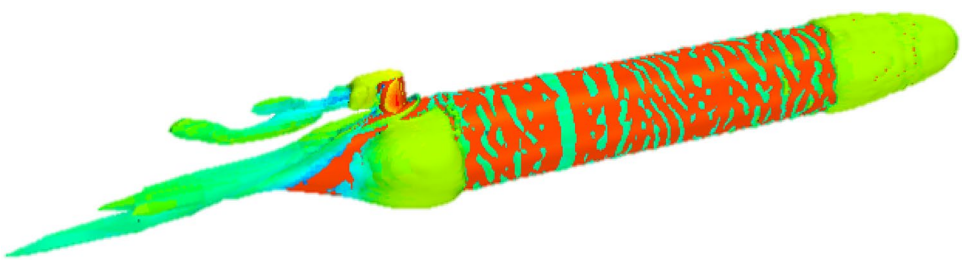

Fig. 7 Unsteady turbulent flow field of the SUBOFF model with appendage ($Q=10$)

Fig. 8 AUV model

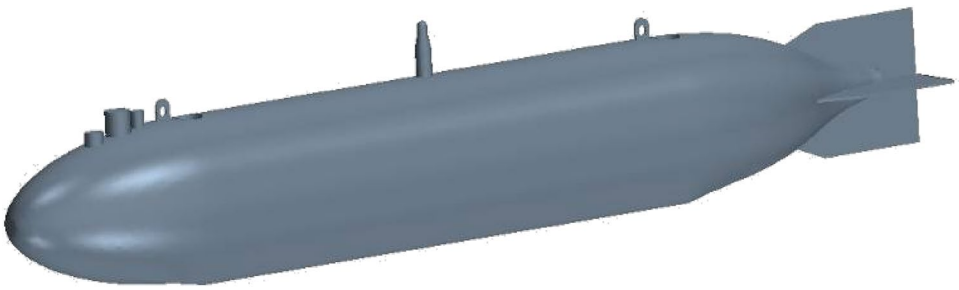

Table 1 Body size and arrangement range of appendages

No.	Appendages	Size and out-reaching height	Arrangement range (m)
1	Sonar 1	Cylinder, diameter 100 mm, height 58 mm	$0 < x < 0.47$
2	Sonar 2	Cylinder, diameter 130 mm, height 117 mm	$0 < x < 3.8$
3	Sonar 3	Cylinder, diameter 70 mm, height 80 mm	$0 < x < 3.8$
4	Lifting ring 1	Width 84 mm, thickness 12 mm, height 108 mm	$0.4 < x < 1.2$
5	Antenna	Maximum diameter 83 mm, height 280 mm	$0 < x < 3.8$
6	Lifting ring 2	Width 84 mm, thickness 12 mm, height 108 mm	$2.6 < x < 3.6$

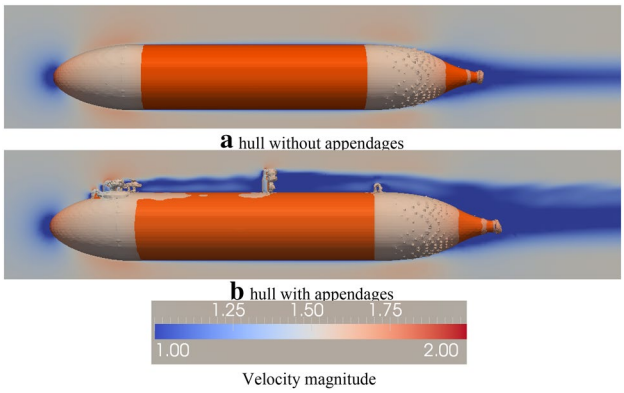

Fig. 9 Flow field comparison between the bare hull and full appendages conditions

Table 2 Drag variation with different appendage arrangement

Arrangement	Drag increment (%)
Bare hull + sonar 1	3.6
Bare hull + sonar 2	11.3
Bare hull + sonar 3	4.6
Bare hull + lifting ring 1	1.7
Bare hull + antenna	16.9
Bare hull + lifting ring 2	1.7
SUM	39.8
Full appendage	43.9

model has six appendages, shown in Fig. 8, including three cylindrical sonar sensors, two rings, and an antenna. Six appendages are separately attached to the bare hull to determine drag increase due to each appendage. Table 1 shows the size, arrangement, and adjustment range of the various appendages, where $x = 0$ shows the location of sonar 1 in Fig. 8. Figure 9 shows the flow field comparison between the bare hull and the full appendage condition when the AUV cruising speed is 1.5 m/s. The colored surface is an isosurface for which $Q = 10$. It reveals that although the size of appendages is much smaller than hull, they have a strong influence on drag increases. The larger the size of the appendages, the more turbulent the flow is, especially when four appendages are arranged near the AUV nose.

First, the direct drag of bare hull with flow speed $u = 1.5$ m/s is calculated, and then the simulation is performed again with an additional appendage added each time. Table 2 shows the increments of direct drag compared to bare hull. The condition with the bare hull and all six appendages are also calculated. Appendages 2 and 5 have the maximum size, so they show greater increments of drag, which reach to 11.3 and 16.9%, respectively. The addition of other appendages leads to relatively small increases in drag, no more than 5%. Calculating the models with different appendages to obtain the drag and accumulate the results, we obtain a total increase of 39.8%. However, when six appendages were placed on the hull, the total drag increased by 43.9%. This indicates that the mutual interference between the appendages does not help to reduce the AUV drag under the current arrangement. The model needs to be optimized to obtain a better arrangement with the least amount of drag.

4.2 Experimental design

To obtain an appendage arrangement with the least drag, theoretically, the optimization algorithm should be combined with the simulation to obtain the optimal solution gradually. However, more than 10 h would be required to obtain a reasonable result for each case. As an alternative, a typical sample could be simulated to reach an approximation model. Further optimization could then be conducted based on this approximation model. This will reduce optimization time significantly. Sample cases were first chosen based on the experimental design. Simulation results will then be calculated to reach an approximation model. The model will reveal the relationship between the arrangement parameters and the total drag.

There are many different experimental design methods, such as random parameter design (RPD) [14], parameter study (PS), central composite design (CCD) [15], orthogonal arrays (OA) [16], uniform design (UD) [17], Latin hypercube design (LHD) [18], and optimal Latin hypercube design (Opt LHD) [19].

In the *i*th particular arrangement plan, the location set of six appendages will be defined to be $x^i = (x_1^i, x_2^i, \ldots, x_6^i)$. According to practical design requirements, in addition to be in the range defined in Table 1, it should also be ensured that

i. Appendage 1 should always be in the front of all the appendages, that is $x_1^i = \min(x_1^i, x_2^i, \ldots, x_6^i)$
ii. The position of two lifting rings should meet $1.86 < \frac{(x_4^i + x_6^i)}{2} < 2.06$
iii. The distance between any two bodies cannot be less than 0.005 m
iv. The vertical height of appendages fixed in the nose section of the hull should be adjusted according to the curve shape, to ensure that they receive adequate exposure.

The RPD method is employed to generate sample points, and parameter sets that do not meet anyone requirement will be filtered. A Python code was developed to generate the parameter set, which ensures that the test space accommodates all of the requirements. The Python code will also calculate drag of 50 parameter combinations. The Python code is responsible for calling the OpenFOAM program that was used to move appendages, generate meshes, conduct the simulation, and read drag values. Figure 10 shows the range of adopted parameter sets. The combination covers the whole range of parameters. Figure 11 is a map of viscous pressure drag C_{dp} and friction drag C_{df} of 50 samples. Within the experimental flow speed, frictional drag varies in a very small range; its

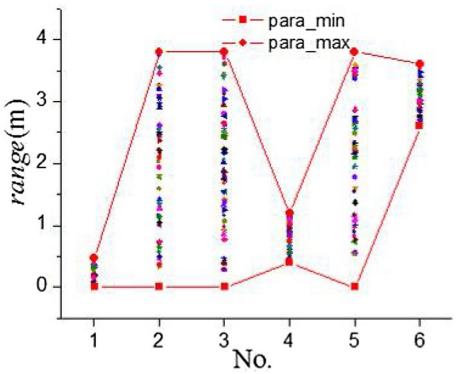

Fig. 10 Range of random parameters

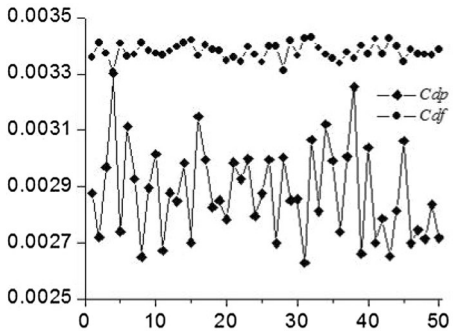

Fig. 11 Variation of friction drag coefficient and pressure drag coefficient

proportion to the total drag is slightly higher than the viscous pressure drag. The maximum viscous pressure drag increases by 25% compared with the minimum condition. The total drag increase corresponds to approximately 10%. It is obvious that a good appendage arrangement layout is beneficial to the navigational range of AUVs. The current AUV arrangement still needs to be optimized so that the drag value may also be decreased. Therefore, we should work for arrangement optimization.

4.3 Arrangement optimization of AUV appendages

A high-accuracy approximation model needs to be constructed between arrangement parameters and their corresponding drag values to make the optimization more reliable. Four types of approximation models are constructed and assessed. They include the response surface method (RSF), radial basis function (RBF) neural network, elliptical basis function (EBF) neural network, and the Kriging model. The model that yields the smallest error is then used as the final approximation model to finish the arrangement optimization. A total of 45 samples were used to construct the approximation model, and the other 5 were used to check the model

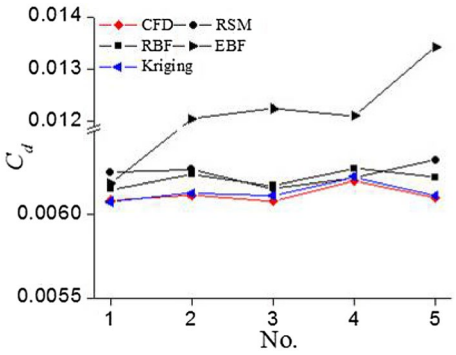

Fig. 12 Accuracy comparison of the four approximation models

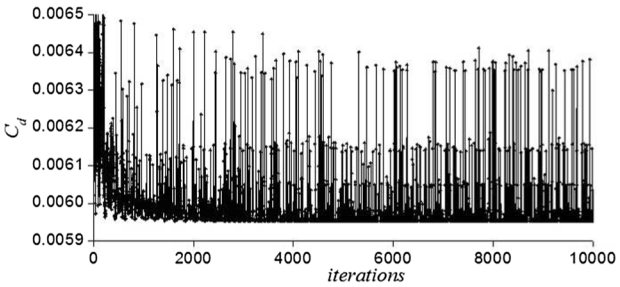

Fig. 13 Optimization of the appendage arrangements based on MIGA

accuracy. Figure 12 shows the comparison between the CFD results and the output values from the approximation models of the five sets. It can be determined that the EBF neural network method shows the worst performance, and that the accuracy of the RBF neural network method is slightly better than the RSF method. The Kriging model has the best accuracy performance overall. This is mainly because the Kriging model honors the actually observed value, weighted moving average algorithm is used to evaluate the value of new position. It has more flexibility than RBF and EBF when dealing with samples, and better performance on local estimation than RSM. Therefore, the Kriging model was adopted as the final optimization method.

4.4 Optimization results

The multi-island genetic algorithm [20, 21] is used as the optimization algorithm in this study. The location set of the appendages $x^i = (x_1^i, x_2^i, \ldots, x_6^i)$ are the input variables, and the output variable is the total drag coefficient, C_d. The number of populations in the algorithm is set to be 10, the size of the population is 20, and the generation of iteration is 50. The optimization process is shown in Fig. 13, which shows that optimization result converges after 3000 steps.

Figure 14 shows the distribution of total drag when changing the position of each appendage according to the optimization result based on the Kriging model. The two lifting rings show very limited impact on the total drag compared with other appendages because of their small size. The location of appendage 1 determines the starting position of the turbulent flow because it is always located at the front of the hull. In addition, the further the starting position is from the hull nose, the more beneficial it is for drag reduction. There are perfect positions for appendages 2, 3, and 5 to reach a minimum drag. Appendage 5 carries the greatest responsibility for the total increase in drag because of its size. Its position also has a major influence. In fact, a small adjustment of appendage 5 could lead to a rapid reduction in the total drag.

To further validate the reliability of the approximation model, the optimized appendage arrangement was simulated with CFD code. The comparison shows that there was a 1.5% error, which is acceptable. Figure 15 shows the flow field comparison between two appendage arrangements; the first is the original arrangement and the second is the optimized arrangement. Obviously, the latter shows less turbulence and thus results in less energy loss. The CFD simulation results indicate a drag reduction of 9.25% after an adjustment of the appendage arrangement. In other words, if the original AUV could complete a 100-km voyage, with the optimized arrangement, the range would be 106 km if all other conditions remained the same. Thus, it is clear that the optimization of an appendage layout can improve the navigational range of an AUV and provide better energy security for its safety and recovery operations.

5 Conclusions and discussion

In this study, the influence of AUV appendages on overall hydrodynamic performance was investigated with specific emphasis on drag reduction. According to the results of the study, the size of appendages installed externally should be as small as possible. If multiple appendages need to be arranged in a practical design, the following conclusions should be considered to improve AUV navigational range. (1) The location of the first appendage should be positioned as far away from the hull nose as possible, to delay the development of turbulence. (2) The largest appendage should always be considered first. (3) Appendages should be arranged in a wide distribution because narrow spaces between appendages may lead to increases in drag. (4) Appendage arrangement optimization should be conducted based on approximation models as time permits.

This paper proposed an optimization procedure for arrangements of AUV appendages. But uncertainty assessment and propagation are not considered at this stage, this may limit the reliability of optimization results to an extent. Our next steps will include consideration of such effect.

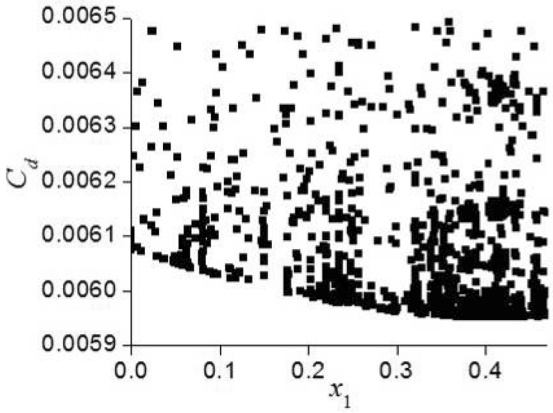

a Trend chart of drag coefficient variation with x_1

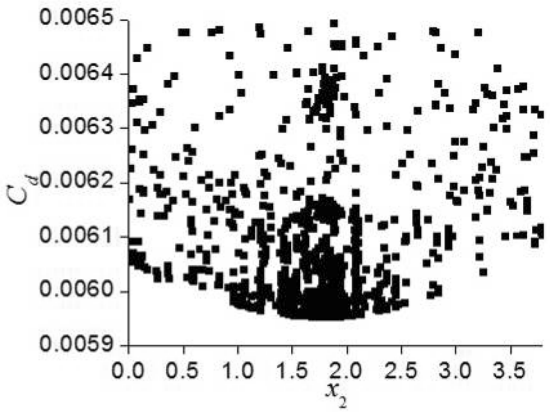

b Trend chart of drag coefficient variation with x_2

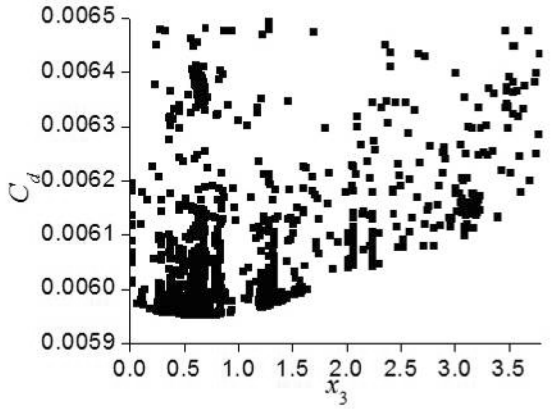

c Trend chart of drag coefficient variation with x_3

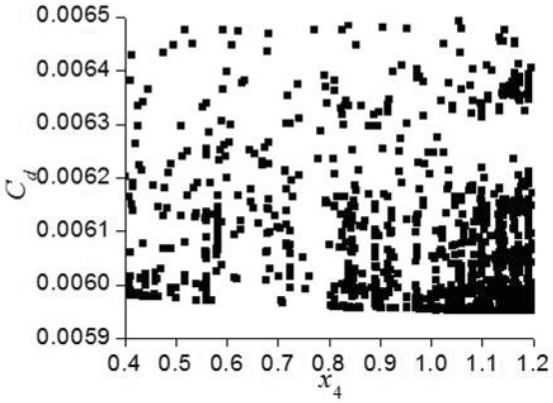

d Trend chart of drag coefficient variation with x_4

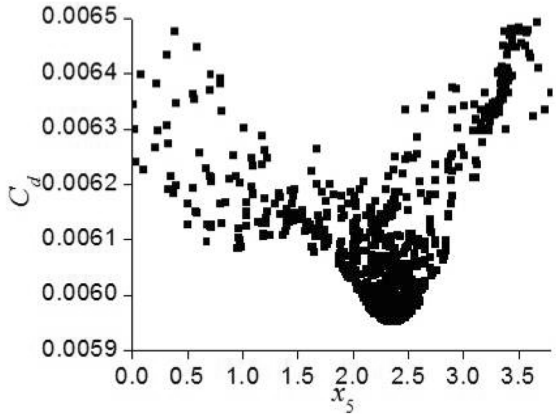

e Trend chart of drag coefficient variation with x_5

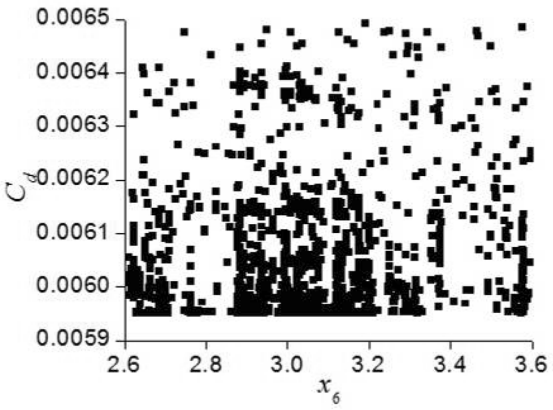

f Trend chart of drag coefficient variation with x_6

Fig. 14 Drag coefficient variation with x_i

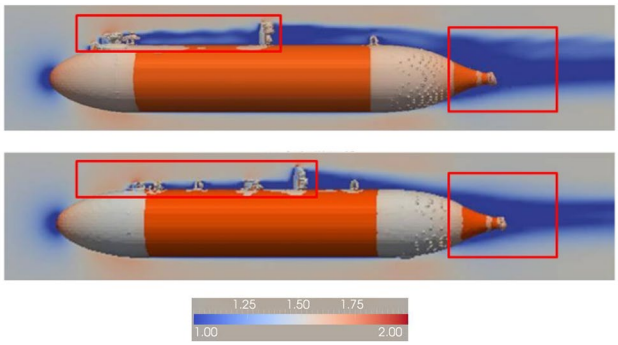

Fig. 15 Comparison of flow field before and after optimization

Acknowledgements This work was supported by The National Key Research and Development Program of China (Grant number 2016YFC0300802), and the State Key Laboratory of Robotics of China (Grant number 2017-Z08).

References

1. Yamamoto I (2015) Research on next autonomous underwater vehicle for longer distance cruising. IFAC-PapersOnLine 48(2):173–176
2. Vasudev K, Sharma R, Bhattacharyya S (2014) A CAGD + CFD integrated optimization model for design of AUVs. In: IEEE OCEANS 2014, TAIPEI, pp 1–8
3. Stevenson P, Furlong M, Dormer D (2007) AUV shapes-combining the practical and hydrodynamic considerations. In: IEEE OCEANS 2007, Europe, pp 1–6
4. Schweyher H, Lutz T, Wagner S (1996) An optimization tool for axisymmetric bodies of minimum drag. In: 2nd international airship conference, Stuttgart/Friedrichshafen, pp 1–8
5. Myring DF (1976) A theoretical study of body drag in subcritical axisymmetric flow. Aeronaut Q 27(3):186–194
6. Gao T et al (2016) Hull shape optimization for autonomous underwater vehicles using CFD. Eng Appl Comput Fluid Mech 10(1):601–609
7. Allen B, Vorus WS, Prestero T (2000) Propulsion system performance enhancements on REMUS AUVs. In: IEEE OCEANS 2000 MTS/IEEE conference and exhibition, pp 1869–1873
8. Groves NC, Huang TT, Chang MS (1989) Geometric characteristics of DARPA suboff models: (DTRC Model Nos. 5470 and 5471). David Taylor Research Center, Bremerton
9. OpenCFD OpenFOAM (2012) The open source CFD toolkit user guide. OpenFOAM Foundation, Dordrecht
10. Wu X et al (2015) An effective CFD approach for marine-vehicle maneuvering simulation based on the hybrid reference frames method. Ocean Eng 109:83–92
11. Dantas JLD, Barros EAd (2013) Numerical analysis of control surface effects on AUV manoeuvrability. Appl Ocean Res 42:168–181
12. Gao T et al (2018) A time-efficient CFD approach for hydrodynamic coefficient determination and model simplification of submarine. Ocean Eng 154:16–26
13. Liu H-L, Huang TT (1998) Summary of DARPA SUBOFF experimental program data. DTIC Document, pp 1–28
14. Wang G et al (2007) Dynamics simulation and optimization of multibody system with random parameters. In: International conference on mechanical engineering and mechanics 2007, pp 1019–1023
15. Ahmadi M et al (2005) Application of the central composite design and response surface methodology to the advanced treatment of olive oil processing wastewater using Fenton's peroxidation. J Hazard Mater 123(1):187–195
16. Hedayat AS, Sloane NJA, Stufken J (1999) Orthogonal arrays: theory and applications. Springer Science & Business Media, Berlin
17. Fang K-T et al (2000) Uniform design: theory and application. Technometrics 42(3):237–248
18. Tang B (2008) Latin hypercube designs. In: Ruggeri F, Kenett RS, Faltin FW (eds) Encyclopedia of statistics in quality and reliability. Wiley, Chichester
19. Park J-S (1994) Optimal latin-hypercube designs for computer experiments. J Stat Plan Inference 39(1):95–111
20. Wang W et al (2011) Parameters optimization of laser shot peening based on multi-island genetic algorithm. Appl Mech Mater 43:387–390
21. Hu X et al (2014) Optimization design of satellite separation systems based on multi-island genetic algorithm. Adv Space Res 53(5):870–876